Subassemblage Cyclic Loading Test of Buckling Restrained Braced RC Frame with Unconstrained Gusset Connections

Zhe Qu,[1] Shoichi Kishiki,[2] Yusuke Maida,[3] and Hiroyasu Sakata[4]

ABSTRACT: An unconstrained gusset connection for buckling restrained braces in reinforced concrete frame structures is proposed and tested as an effort to mitigate the complicated and usually harmful interactions between the steel gusset plate and the adjoining reinforced concrete column. Local damage control incorporating the rearrangement of beam flexural strength is also proposed to enhance the reliability of the gusset connection by moving the potential plastic hinge of the beam away from the connection region. Two different connecting methods, one with post-tensioned steel rods and the other embedded stud groups, were considered. The results of the cyclic loading tests on RC beam-gusset connection subassemblies confirmed that both connecting methods are available as long as the local damage control is implemented, which is not only helpful in eliminating the unfavorable deformation loss at the connection, but more importantly, can prevent the BRBs from being dislocated as a result of the beam end failure in extreme earthquake events.

INTRODUCTION

Buckling restrained braces (BRBs) were first developed in the 1980s in Japan as energy-dissipating braces to provide seismic protection for steel moment-resisting frames (Watanabe et al. 1988). Its application has since then been extended to reinforced concrete (RC) frames, primarily for seismic retrofit of existing multi-story buildings. As for the methods of connecting BRBs to existing RC components, engineers used to install buckling-restrained braced steel frames rather than individual BRBs in order to distribute the force transfer between the BRBs and the RC components. The retrofitting braced steel frames are either attached to the building façade or installed within the RC frame (e.g., Brown et al. 2001, Ishimura et al. 2012). In both cases dense post-installed anchors on the RC-steel frame interface are usually required for integrity, making the construction noisy, dusty and time consuming. Various improvements have been proposed to reduce the number of post-installed anchors to ease the construction (e.g., Harayama et al. 2012, Ishimura et al. 2011).

For new RC constructions, it is possible to embed extensions of the gusset plate of a BRB in the RC components, making the connection more compact and easier-to-construct (e.g., Ogawa et al. 2004, Gu et al. 2011). However, the steel gusset plate, which is usually fastened to both the adjoining RC column and the beam end, need to be strong and stiff to prevent out-of-plane buckling, and would have detrimental effects on the seismic performance of the adjoining RC column (Kishiki et al. 2008). For example, it may reduce the slenderness and thus increase the risk of shear failure of the RC columns. It may also increase the stiffness of the RC bare frame and thus increase the proportion of base shear force that is carried by it. This increased shear force may not have been appropriately addressed in the design of the RC frame because the extra stiffness due to the gusset plate is usually not taken into account in a structural analysis.

Rather than connecting to both the columns and beams, some researchers have examined the possibility of fastening BRBs to only the RC beams. In the method proposed and tested by Ishii et al. (2004), the BRB gusset plate is fastened to the side surface of RC beams by pre-tensioned steel rods which penetrate the web of the beam. As observed in their test, the damage of the underneath concrete would considerably impair the effectiveness of the connection and thus reduce the energy dissipation of BRBs when such a connection is placed at the beam end, where plastic hinges are expected. Yokouchi et al. (2004) also installed the gusset plates of energy-dissipating braces to the side surface of RC beams in their pseudo dynamic test of a full-scale retrofitted RC frame building in Japan. Similar problems can be expected in their application.

Berman and Bruneau (2009) proposed an 'unconstrained gusset connection' for BRBs in steel frames, in which the gusset plate is bolted to the steel beam end and separated from the steel column by an

[1]Associate researcher, Key Laboratory of Earthquake Engineering and Engineering Vibration, Institute of Engineering Mechanics, China Earthquake Administration, No.1, North Waihuan Road, Yanjiao, Sanhe, Hebei 065201, China.

[2]Associate professor, Structural Engineering Research Center, Tokyo Institute of Technology, Nagatsuta, Midori, Yokohama, 226-8503, Japan.

[3]Assistant professor, Graduate School of Engineering, Department of Architecture, Chiba University, 1-33 Yayoi-cho, Inage-ku, Chiba, 263-8522, Japan.

[4]Professor, Tokyo Institute of Technology, Ookayama, Meguro, Tokyo 152-8552, Japan.

intended gap. In the present study, this idea is tried out for BRBs in RC frames through experimental investigations. To address the problems encountered by Ishii et al. (2004), a 'damage control' scheme is proposed for the local connection region in which the RC beam end that receives the unconstrained BRB gusset is expected to remain free of damage, even if the structure is subjected to major earthquakes. In particular, the potential plastic hinge that usually occurs at the RC beam end is expected to be relocated to outside the gusset connection region (i.e., forward to the center of the span). This is similar in concept to the reduced beam sections (RBS) in steel moment-resisting frames (Jones et al. 2002, ANSI/AISC 2010).

UNCONSTRAINED GUSSET CONNECTIONS

Connection details

The proposed connection is referred to as 'unconstrained gusset connection' because the gusset plate is not constrained by the RC column and is fastened only to the beam. A gap of w_{gap} wide separates the gusset plate from the column to prevent it from touching the column surface even if the structure sustains large lateral drift (Figure 1). It is not necessary for the center line of the BRB to pass through the center of the beam-to-column joint. Rather, it is preferred to offset the center line of the BRB by an eccentricity, e, to allow for a more compact gusset plate. Two different connection details were proposed. One uses post-tensioned steel rods to fasten the gusset plate on top surface of the beam (denoted as PT type hereinafter, Figure 1(a)) and in the other case, extensions of the gusset plates are embedded within the underneath concrete beam (denoted as EB type hereinafter, Figure 1(b)).

For the PT type, high-strength steel rods go through the beam and are post-tensioned to fasten the base plate of the gusset on the beam. The shear force on the gusset plate is resisted by the friction between the base plate and the concrete surface, while the tensile force is resisted by post-tensioning of the steel rods. Because both friction action and post-tensioned rods exhibits very high stiffness, such a connection is expected to be very stiff.

For the EB type, the gusset plate extends into the beam and is anchored there by headed stud groups on both sides of the embedded plate. The embedment does not go into the beam- column joint to ease the load transfer as well as avoid hindrance to the joint reinforcement. Rather than making holes on the embedded plate to give way to closed stirrups, open stirrups with 135° hooks as shown in Figure 1(b) are used for easier construction. Since the embedded plate can contribute a lot to the shear strength of the concrete beam within the embedment region, the amount of stirrups in this segment are not critical to the shear design of the beam.

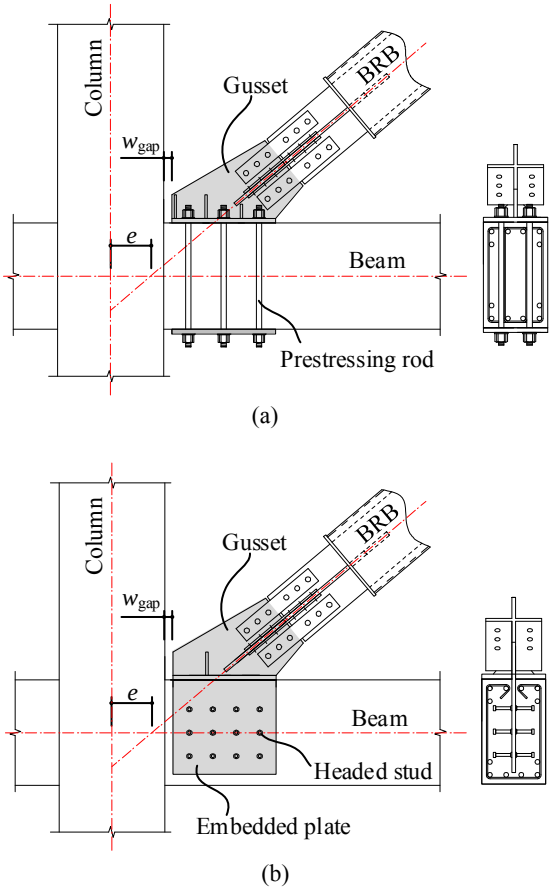

Fig. 1. Proposed unconstrained gusset connections: (a) post-tensioned type (PT) and (b) embedded plate type (EB).

Damage control at beam end

The overlap of BRB connections and potential plastic hinges is unfavorable for the performance of the connection. To make it worse, shear failure may occur at the beam end section immediately outside the beam-to-column joint if the beam yields at this section and at the same time is subjected to large shear and tensile force from the brace. Such shear failure at the beam end could be fatal to the whole braced frame system because the braces would be dislocated from the rest of the structural system. In addition, the large tensile force on the beam end section will also reduce the yield strength of the beam

To address these concerns, special focus was given to controlling of the plastic hinge location of the beam. The beam longitudinal rebars are re-arranged to adjust the flexural strength of the different segments of the beam to move the plastic hinge outside the beam segment that receives the gusset plate. As shown in Figure 2, the braced beam without such 'damage control' (DC) (Figure 2(b)) has the same longitudinal reinforcement as a bare frame beam (Figure 2(a)), which is expected to yield at the end (i.e., Section I) under major earthquakes. In this case, the yield force, V_{By}, of the braced beam is

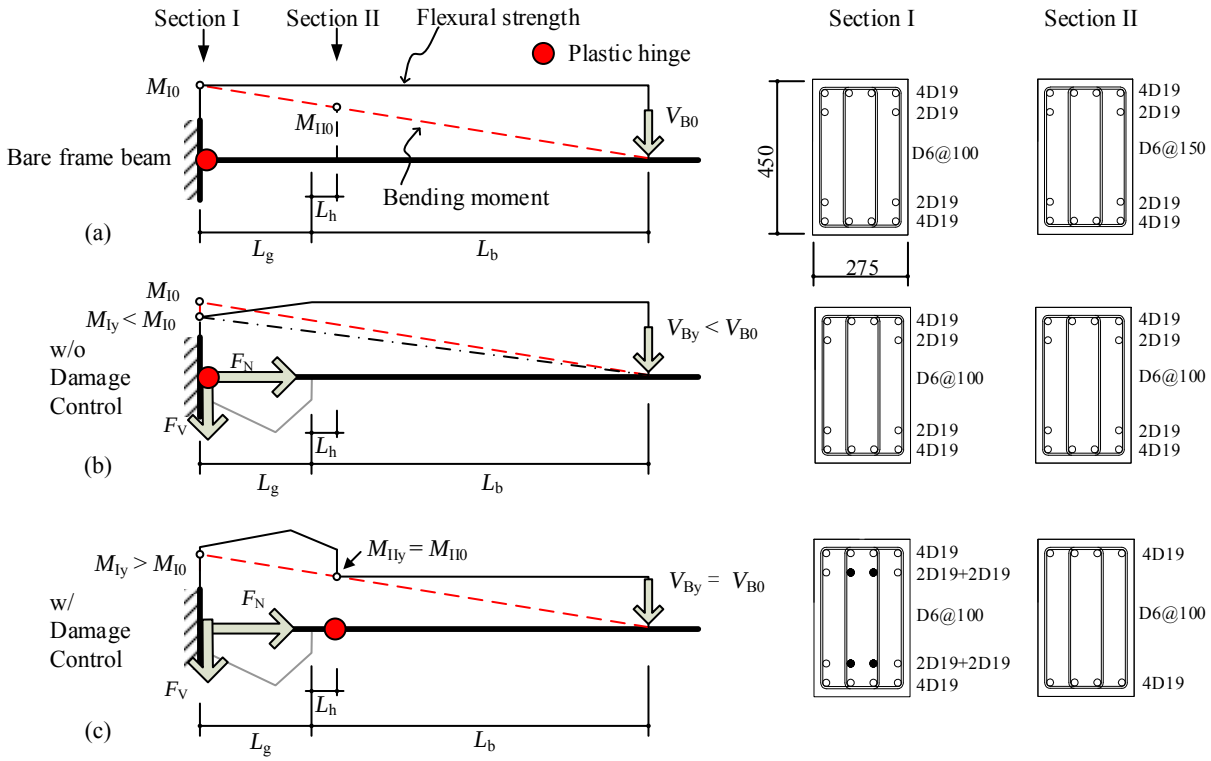

Fig. 2. Control of beam plastic hinge location: (a) Bare beam, (b) braced beam without damage control and (c) braced beam with damage control.

likely to be less than that of a bare frame beam, V_{B0}, because the flexural strength at Section I is reduced from M_{I0} to M_{Iy} by the effect of the tensile force, F_N, of the brace.

The plastic hinge can be moved to Section II if the amount of rebars there is reduced and that at Section I is increased so that the flexural strength $M_{IIy} = M_{II0}$ and $M_{Iy} > M_{I0}$, where M_{II0} is the moment at Section II when M_{I0} is reached at Section I (Figure 2(c)). Section II is offset by L_h outside the gusset connection region. In such a manner, the beam yield force, V_{By}, remains equal to V_{B0}. More importantly, the beam segment between Section I and II would keep essentially elastic and free of damage so that the brace can work well with the rest of the system even if the beam segment outside the gusset connection is heavily damaged.

TEST PROGRAM

Specimens and test setup

The unconstrained gusset connection with the damage control scheme is examined through subassemblage cyclic loading tests. A full-scale half-span cantilever beam with a brace connection was separated from the archetype buckling restrained braced frame (BRBF) subassembly shown in Figure 3(a), which consists of a column extending half the story height above and below the joint, a beam extending half a span length both sides of the joint, and a BRB connected to the beam. The dimensions of the subassembly were partly dependent on the available test facility. For simplicity of the loading setup, the cantilever beams were rotated 90° and cast into RC stubs at the bottom, which were fastened to the lab's strong floor through six post-tensioned steel rods and was blocked by a pair of steel shear keys on both sides (Figure 4).

The clear half-span length of the tested beam (from the column surface) was 1800 mm and the beam cross sectional depth was 450 mm, yielding a typical flexural beam of shear span-to-depth ratio of 4. The inclination angle of the brace was 40° and the brace axis was intersected with the beam axis at 85 mm inside the beam-to-column joint (i.e., the stub in the test). Assuming that the column cross section is also 450 mm in depth, this indicates a 140 mm offset of the brace center line from the center of the beam-to-column joint. The base plate of the gusset plate was 440 mm long and placed w_{gap} = 10 mm away from the stub surface to keep the gusset plate clear of the stub surface even if the beam sustains as large as 10% chord rotation.

The beam free end (i.e. the upper end in the test setup) was driven by two 200 kN displacement-controlled actuators in parallel. Instead of using real BRBs, a 1000 kN force-controlled actuator was used to simulate the brace axial force on the gusset plate. The nominal strength of the BRB in test was assumed to be 500 kN, which is about 1/30 of the axial compressive strength of a 450 by 450 mm RC column cross section of 70 MPa concrete.

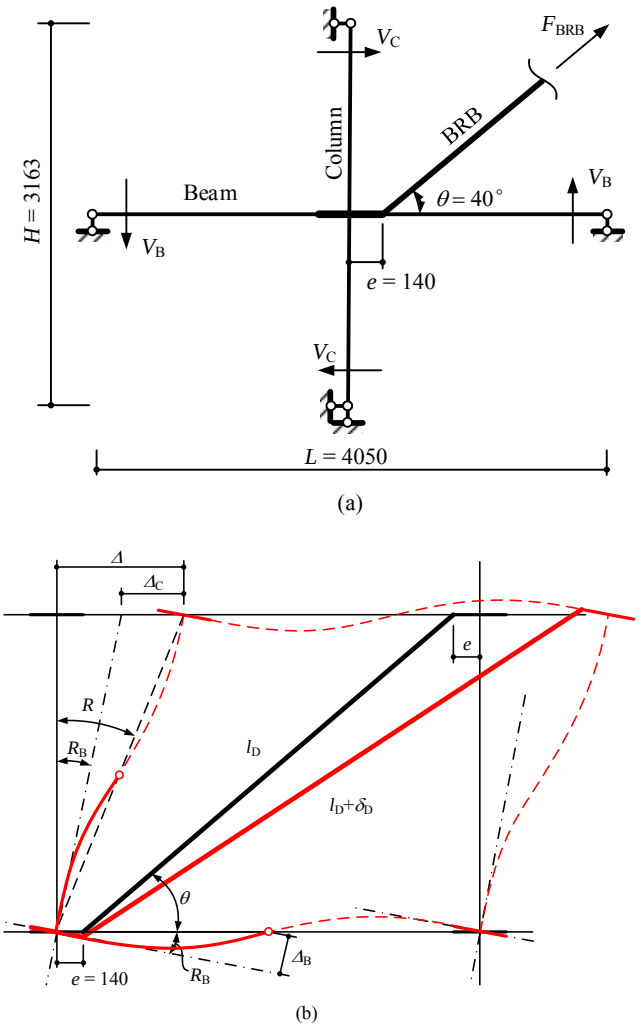

Fig. 3. Subassemblage of buckling restrained braced frame: (a) un-deformed and (b) deformed configuration.

The combination of two types of connection details and two sets of beam reinforcement leads to four specimens of braced beams. A bare beam was also included as the control specimen. Therefore, a total of five specimens were tested by the above setup (Table 1). The beam cross section was 450 mm by 275 mm. The flexural reinforcement ratio of the bare beam (No.1) and the braced beam without damage control (No.2 and 3) was about 1.6% for the whole length of the beam (Figure 2a and 2b), while that of the braced beam with damage control (No.4 and No.5) was 2.2% within the $L_g + L_h = 550$ mm distance from the fixed end and reduced to 1.0 % in the rest of the beam (Figure 2c). Cast iron mechanical anchors were used to terminate the longitudinal rebars in the specimens with damage control. The stirrups were also slightly varied corresponding to the locations of potential plastic hinge. For the concrete properties, three suites of 150 by 300-mm concrete cylinders were tested during the subassemblage tests (Table 1). Each suite consists of three cylinders for the compressive strength and another three cylinders for the elastic modulus.

For the PT type connections, six high-strength steel rods of 21 mm diameter were post-tensioned to 2/3 the nominal yield strength, that is, 375 kN per rod, to provide an overall post-tensioning force $P_0 = 1500$ kN to fasten the gusset plate. This was determined by satisfying Equation (1) with about 20% safety margin so that the gusset plate would not slip along the interface under the nominal BRB axial force, F_m, of 500 kN. Such a post-tensioning force subjected the underneath concrete to a normal pressure of about 12 MPa at the same time.

$$\mu(P_0 - F_m \sin 40°) > F_m \cos 40° \qquad (1)$$

where μ is the friction coefficient of concrete-to-steel interface and was taken as 0.4 in light of the extensive experimental investigations by Rabbat and Russell (1985) and Baltay and Gjelsvik (1990), which suggest that a $\mu = 0.4$ can be adopted with confidence when the normal pressure is within 1~20 MPa.

For the EB type specimens, 12 ϕ16 headed studs of 80 mm long and a 235 MPa nominal yield strength were welded on each side of the embedded plate for anchorage. The layout of the stud group was a 3×4 array at 100 mm spacing both ways. The geometric center of the stud group was offset by about 200 mm from the axis of the BRB (see Figure 1b). The strength of the stud group was checked to withstand the combined shear and eccentric moment induced by the eccentric BRB axial force, F_B. An approximate method was employed to estimate the shear force carried by each stud in the group, which assumes that the center of rigidity of the stud group remains at its geometric center and the embedded plate beneath the stud group is rigid. The shear strength of a single stud was calculated by Equation (2) proposed by Ollgaard et al (1971).

$$q_s = 0.5 A_{sc} \min\left(\sqrt{f_c E_c}, 900\right) \qquad (2)$$

where A_{sc} is the cross sectional area of the stud; f_c and E_c is the concrete compressive strength and elastic modulus, respectively (in MPa).

Load control

Cyclic static loading was performed with gradually increased story drift amplitudes listed in Table 2. The first two loading cycles had drift ratio amplitude of 1/400, during which the brace was expected to slightly yield while the beam remained essentially elastic. This was followed by load cycles of 1/200 and 1/100 story drift ratio, which generally correspond to the ‘damage limit state’ and ‘ultimate limit state’ of buildings protected by specific energy dissipating devices (e.g., BRBs) in Japan, respectively (JSSI 2007). Two cycles of loading were performed for each story drift amplitude. Finally, a load cycle of 1/50 story drift ratio was performed to confirm the behavior of the specimen under large

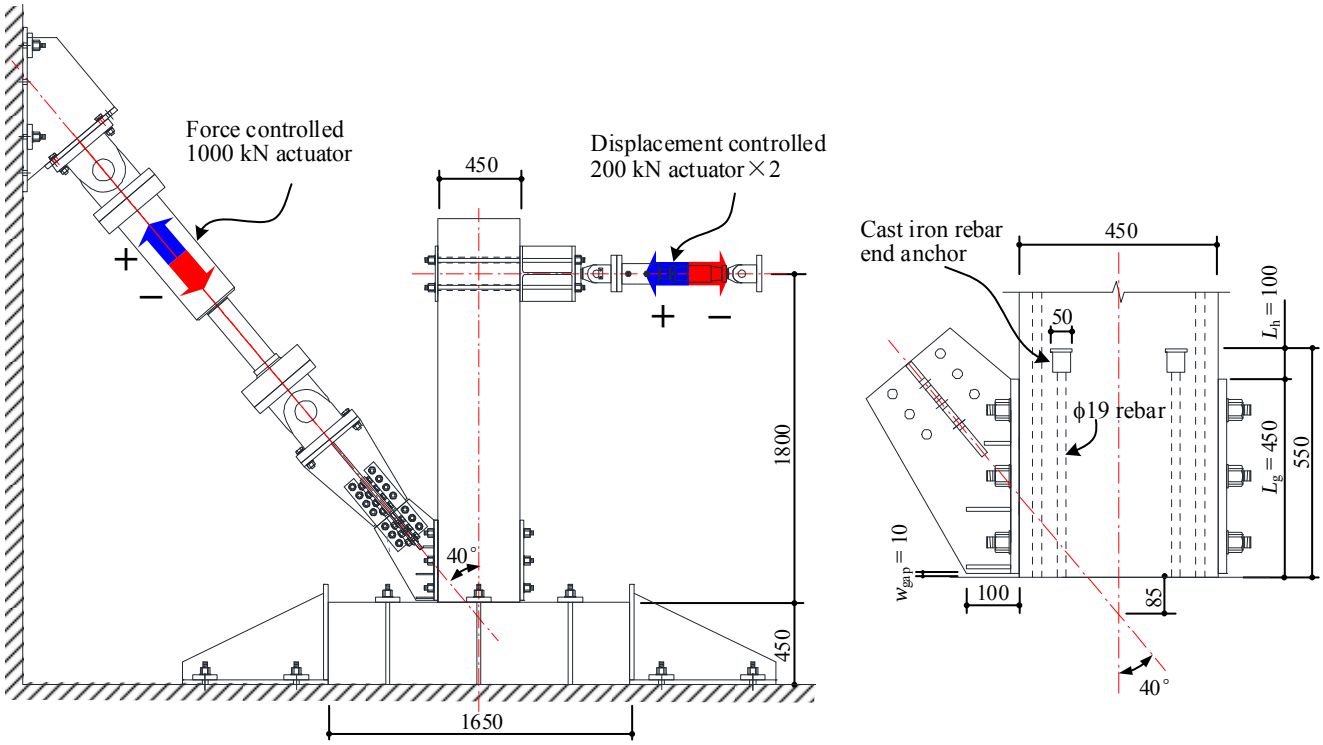

Fig. 4. Test setup and dimensions (length unit: mm).

Table 1. Specimen properties.

Specimen	No.1 (Bare)	No.2	No.3	No.4	No.5
Connecting method	-	PT	EB	PT	EB
Stud	-	-	24ϕ16	-	24ϕ16
Post-tensioned rod	-	6ϕ21 (C)	-	6ϕ21 (C)	-
Post-tensioning force (kN)	-	1489.6	-	1466.5	-
Damage control	-	No	No	Yes	Yes
Concrete compressive strength (MPa)*	70.7	70.7	70.0	70.7	71.4
Concrete elastic modulus (MPa)**	42648	42648	39333	42648	36996

* obtained by compression tests on 150 by 300-mm concrete cylinders.

deformations. After the 1/50 load cycle, the specimen was pushed monotonically towards the positive direction to full stroke of the horizontal actuators.

Table 2. Loading protocol.

Story drift ratio	1/400	1/200	1/100	1/50
Number of cycles	2	2	2	1

The loading procedure represents a simplified version of a substructure hybrid test of the previously described subassembly in Figure 4(a). Specifically, the half-span beam and the local connection in the archetype subassembly were represented by physical models (i.e., the specimens) while the brace and the column were represented by simple numerical models. The column was assumed to remain elastic throughout the loading process so that its behavior can be described by the linear function in Equation (3).

$$\Delta_C = \frac{V_C}{K_C} = \frac{V_C}{12E_cI_C/H^3} \tag{3}$$

where Δ_C is the column drift (part of the story drift, see Figure 4(b)); V_C is the column shear force and $K_C = 12E_CI_C/H^3$ is the column flexural stiffness. I_C is the the moment of inertia of the assumed 450 mm × 450 mm column cross section; H =3163 mm is the story height.

The hysteresis of the BRB was assumed to be elastic-perfectly plastic as described in Equation (4), which is the simplest while acceptable model for a yielding component. To have constant BRB force in a wide range of the loading process makes the load control of the virtual BRB much easier. In addition, it allows for an easy separation of the effects of the BRB force and the RC beam deformation on the behavior of the gusset connection. A diagonal force-

controlled actuator was connected to the gusset plate to apply the hysteretic force of the BRB.

$$F_{BRB} = \min\left(K_{BRB}\delta_{BRB},\ F_m\right) \quad \text{during first loading} \tag{4a}$$

$$F_{BRB} = \max\left(F_m - K_{BRB}\left|\delta_U - \delta_{BRB}\right|,\ -F_m\right) \quad \text{during unloading and reloading} \tag{4b}$$

where F_{BRB} and δ_{BRB} is the BRB axial force and deformation, respectively; F_m = 500 kN is the BRB nominal strength; K_{BRB} = 139 kN/mm is the BRB axial stiffness; δ_U is the BRB deformation at the last onset of unloading.

Besides the assumed mechanical behavior of the imaginary part of the subassemblage, the following relationships of force equilibrium and geometric compatibility were also necessary to complete the substructure model. The moment equilibrium around the center of the beam-to-column joint of the subassemblage in Figure 4(a) is given in Equation (5).

$$V_C H = V_B L + F_{BRB} e \sin\theta \tag{5}$$

where L = 4050 mm is the span length; e = 140 mm is the eccentricity of the axis of BRB with regard to the center of the beam-to-column joint; θ = 40° is the inclination angle of the BRB.

By the geometric compatibility of the deformed frame subassemblage, the relationship between the axial deformation of the BRB, δ_{BRB}, and the story drift ratio, R, can be derived as Equation (6) and (7).

$$R = \frac{\Delta}{H} = \frac{R_B H + \Delta_C}{H} \tag{6}$$

$$\delta_{BRB} = RH\cos\theta + 2R_B e\sin\theta - 2\delta_L \tag{7}$$

where Δ is the overall story drift, including the drifts due to column deformation and joint rotation; R_B = $2\Delta_B/L$ is the beam chord rotation and δ_L is the deformation loss at the BRB gusset connection.

Equation (3) to (7) provides the basis of the test load control. Many parameters in these equations were known before the test, e.g., the dimensions of the subassemblage, H, L, e, θ, the stiffness of the column, K_C; the BRB initial stiffness and the nominal strength, K_{BRB} and F_m. Some variables were measured during the loading process, such as the beam shear force, V_B, the BRB axial force, F_{BRB}, the deformation loss, δ_L, and the BRB unloading deformation δ_U. Other variables such as the story drift ratio, R, and the column shear force, V_C, were derived from the other prescribed or measured quantities.

In each load increment, the beam was first loaded to a target displacement, Δ_B, and the corresponding target force of the BRB was calculated through the above equations following the procedure in Figure 5. The force in the virtual brace (the diagonal actuator), F_{BRB}, was then adjusted to its target force. F_{BRB} is part of the moment equilibrium in Equation (5) and has a direct effect on determining the target force. In addition, any change of F_{BRB} may also have effects on some other measured variables such as δ_L and Δ_B. As a result, the adjusting of F_{BRB} was an iterative process until the actual force of the diagonal actuator matched the target force. Because most of the above equations represent linear relationship, and F_{BRB} was assumed to keep constant after the BRB yields, the iterative process was easy to converge.

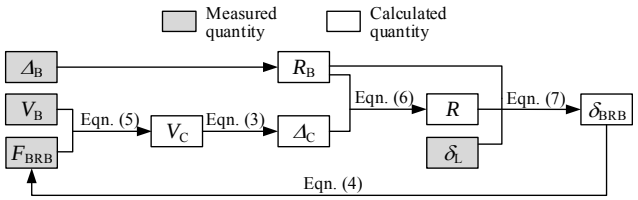

Fig. 5. Flowchart of load control process in a single load increment.

TEST RESULTS

RC Beams

The hysteresis of beam shear force, V_B, and chord rotation, R_B, is plotted in Figure 6. For comparison, skeleton curves calculated by Response 2000 (Bentz 2000) are also depicted. For Specimen No.2 and No.3, the calculated skeleton curves taking into account the effects of axial force, F_N, on the cross section are also overlaid.

The calculated skeleton curves match well with the test results for Specimen No.1, where there is no axial force on the beam cross section. As expected, the flexural strength of Specimen No.4 and No5, where damage control (DC) scheme was applied, is almost identical to Specimen No.1. By comparing with the calculated skeleton curves, the increase of strength in the negative loading of Specimen No.2 and No.3 can be well explained by the effect of the axial compressive force on the beam section, while on the other hand, the expected strength decrease in the positive loading when the beam end was supposed to carry axial tensile force was not observed in the test.

The frame story drift ratios, R, at the beam yielding and the corresponding beam chord rotations, R_B, are compared with the frame story drift ratios at the first yielding of the imaginary BRBs in Table 3. The beam yielding was defined by the yielding of the outermost longitudinal rebar. Despite the differences in connection details and beam reinforcement, the BRB yielded at much smaller story drift than the RC beam did. The maximum beam chord rotations achieved in the test are also listed in Table 3. These are merely the beam deformations when the loading

was terminated because the horizontal actuators were out of the stroke, with the exception of Specimen No.3, for which the deformation when the beam shear dropped to 85% of the maximum shear was listed.

In Figure 7, the damages of the RC beams are summarized in terms of apparent cracks and strain distributions of the longitudinal rebars. The beam in Specimen No.1 is an ordinary cantilever RC beam which yielded at the fixed end. Major cracks (e.g., those wider than 0.2 mm) on the beam surface clearly indicated a plastic hinge at the fixed end, while some major cracks were wide spread along the beam.

For Specimen No.2 and No.3, the beams also yielded at the fixed end during the positive loading. During negative loading, however, they yielded at both the fixed end and the section immediately outside the gusset plate. Major cracks of Specimen No.3 (EB) spread widely into the gusset plate region while those of No.2 (PT) were much constrained near the beam-to-column interface because of the pre-stressing of the concrete underneath the gusset plate.

For Specimen No.4 and No.5 in which the beam reinforcement is adjusted to perform damage control, the longitudinal rebars only yielded at sections outside the gusset plate region and major cracks were also concentrated there, indicating that the plastic hinges of the beams were successfully moved outside the connection region. Because of the pre-stress of the concrete, the cracks within the connection region in Specimen No.4 (PT+DC) were much less than those in No.5 (EB+DC) and were almost perpendicular to the beam axis.

By relocating the plastic hinge, the hysteretic energy dissipated by the RC beams was not much affected. This can be seen from the traditional equivalent damping ratios in Table 3. The equivalent damping ratio is calculated as $\zeta_{eq}=E_D/(2\pi ku^2)$, where E_D is the hysteretic energy in a complete load cycle, k is the secant stiffness at the maximum deformation, u. At extreme events, the beam end may sustain severe damage at the potential plastic hinge, and the beam may even detach from the column if such damage is concentrated at the beam-to-column surface, considering that the BRB may at the same time impose significant tensile and shear force on that surface. By moving the potential plastic hinge outside the connection region and away from the column, the load condition for the plastic hinge becomes less critical and thus the risk of sudden failure of the beam can be mitigated. Besides, even if the beams fail during extreme events, the BRB will not be dislocated together with the beam and the structural integrity can be retained.

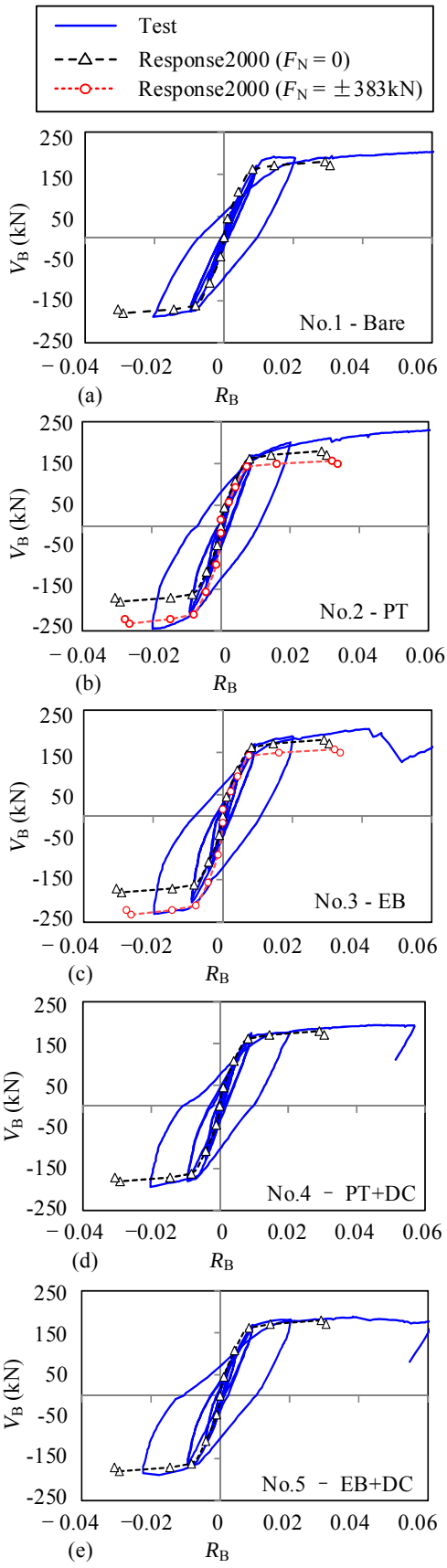

FIG. 6. Shear force and chord rotation of RC beam: (a) Specimen No.1; (b) No.2; (c) No.3; (d) No.4 and (e) No.5.

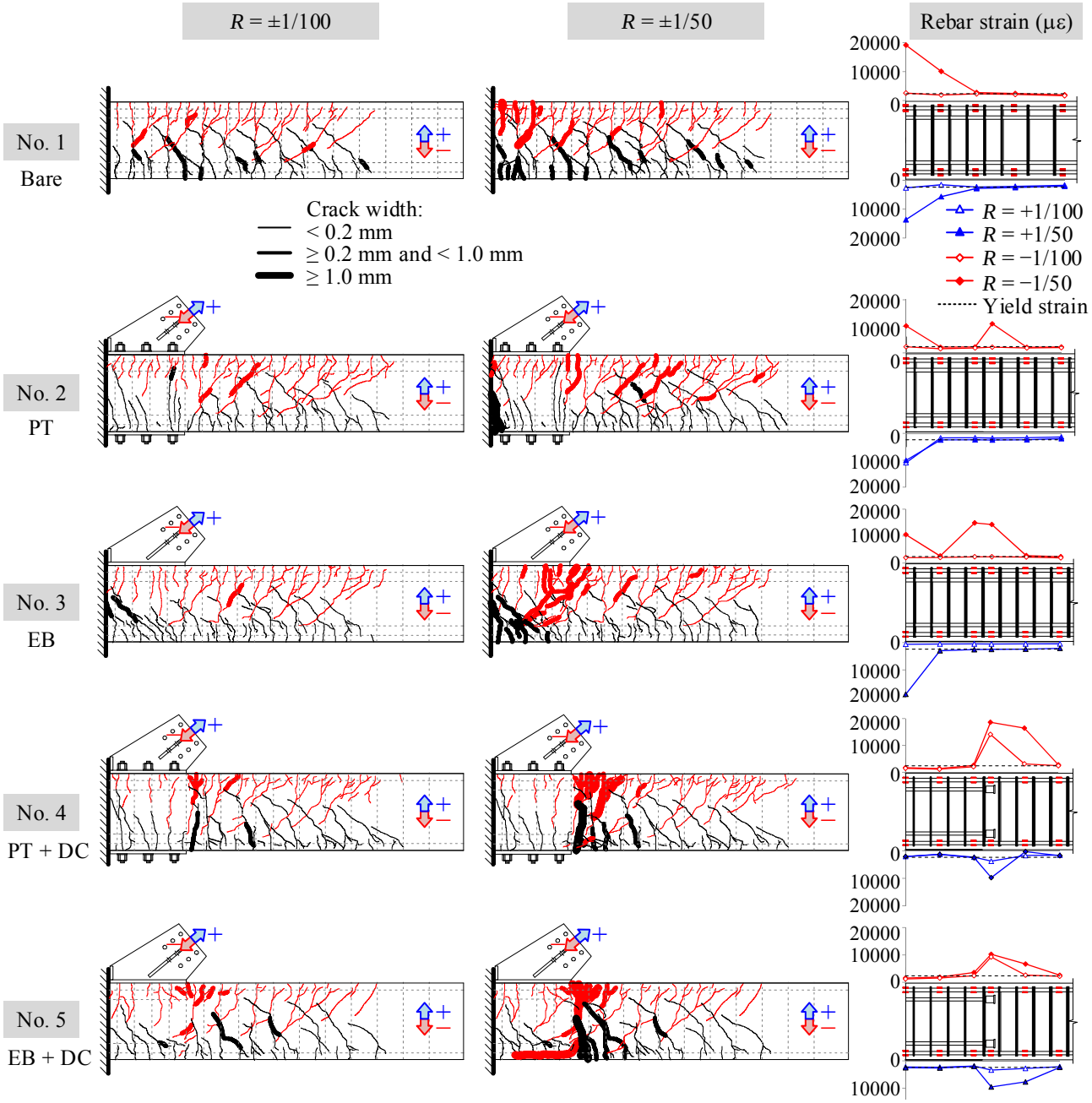

FIG. 7. Damage to RC beams.

Table 3. Characteristic deformations and energy dissipation of RC beams.

	No.1 (Bare)	No.2 (PT)	No.3 (EB)	No.4 (PT+DC)	No.5 (EB+DC)
Story drift R at BRB yields	-	1/686	1/651	1/620	1/635
Story drift R at beam yields	+1/111 (-1/104)	+1/145 (-1/125)	+1/124 (-1/131)	+1/115 (-1/140)	+1/117 (-1/136)
Beam chord rotation R_B at beam yields	+1/119 (-1/112)	+1/165 (-1/134)	+1/137 (-1/158)	+1/127 (-1/165)	+1/128 (-1/155)
Beam chord rotation at the end of the monotonic push	1/15	1/15	1/21*	1/17	1/16
Equivalent damping ratio for the 1/50 load cycle	19.5%	22.4%	23.3%	23.7%	24.1%

* Beam chord rotation when the beam shear was decreased to 85% of the maximum beam shear.

Deformation Loss at Gusset Connections

To concentrate the deformation in the plastic segment of a BRB, the connection is preferred to exhibit as small deformation as possible. Such deformation is a major source of the deformation loss in terms of the BRB efficiency. In the present test, it was monitored by an LVDT as denoted by δ_L in Figure 8, which represents the deformation at the connection (or separation) between the concrete and the gusset plate.

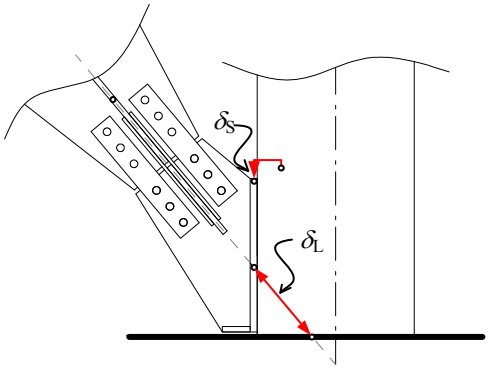

FIG. 8. Measurement for deformation loss at gusset connection.

The concentrated force imposed by BRB on the gusset plate is a direct but not the only source of δ_L. Since the RC beam end to which the gusset plate is connected is by no means perfectly rigid and is subjected to cyclic loading in addition to the BRB force, it has more or less some effect on the behavior of the gusset connection when it deforms, especially when it sustains nonlinearity. Taking Specimen No.2 for example, the variation of the deformation loss, δ_L, is compared with the story drift ratio and the BRB hysteresis (imaginary in the test) side by side in Figure 9 for two selected load cycles. Each cycle starts from Point A, where the beam shear is zero and the BRB undergoes yielding in tension. It then goes successively through Point B corresponding to the positive peak story drift for the current load cycle; Point C where the BRB yields in compression while the beam shear is decreased; Point D at the negative peak story drift; and Point E where the BRB yields in tension again and the RC beam is partially unloaded.

During the 1/100 load cycle, the RC beam remained essentially elastic and the deformation loss is strongly related to the variation of the BRB force. Specifically, the deformation loss underwent substantial decrease when the BRB force was changed from the tensile to the compressive strengths (i.e., from Point B to C in Figure 9(a)) and later was significantly increased from D to E when the BRB tensile force was restored.

Although not very significant, variation in the deformation loss while the BRB force kept constant can also be observed during the 1/100 load cycle, which was accompanied by the loading and unloading of the RC beam. Such an effect became more significant when the RC beam was extensively yielded during the 1/50 load cycle (see Figure 9(b)). The deformation loss kept almost constant when the RC beam was in its elastic loading branch and the BRB force kept constant (i.e., from point A to X in Figure 9(b)). After the RC beam yielded at point X, the deformation loss exhibited a sudden increase while the BRB force still kept constant (i.e., from point X to B). The same phenomenon can be observed at the yield point Y in the opposite direction, beyond which the deformation loss increased considerably from point Y to D.

It is therefore evident that the nonlinearity of the RC beam ends was a considerable source of deformation loss in the specimens without damage control (DC) scheme. For Specimen No.2, the maximum deformation loss was increased from 0.7 mm during the 1/100 load cycle to 2.7 mm during the 1/50 load cycle. By contrary, the deformation loss kept well below 0.3 mm up to the 1/50 load cycle in the companion Specimen No. 4 with DC. Similar effect of suppressing the growth of deformation loss through damage control can also be found by comparing Specimen No.3 and No.5 (see Table 4 and Figure 10).

Table 4. Maximum deformation loss up to 1/50 load cycle (mm).

	No.2 (PT)	No.3 (EB)	No.4 (PT+DC)	No.5 (EB+DC)
1/100 load cycle	0.7	1.4	0.1	1.2
1/50 load cycle	2.7	3.6	0.2	1.4

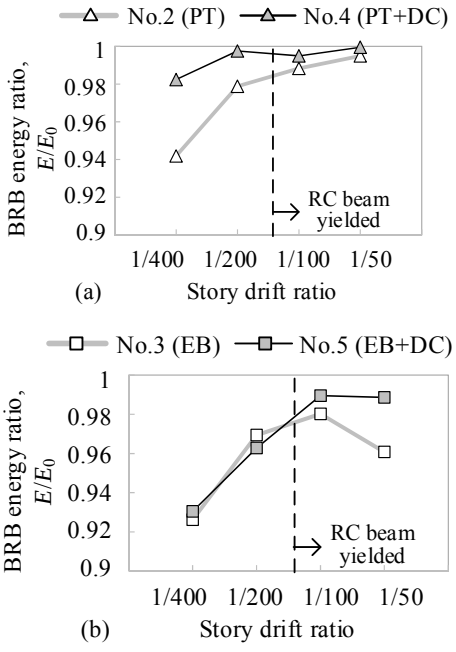

FIG. 11. BRB energy ratio: (a) PT specimens and (b) EB specimens.

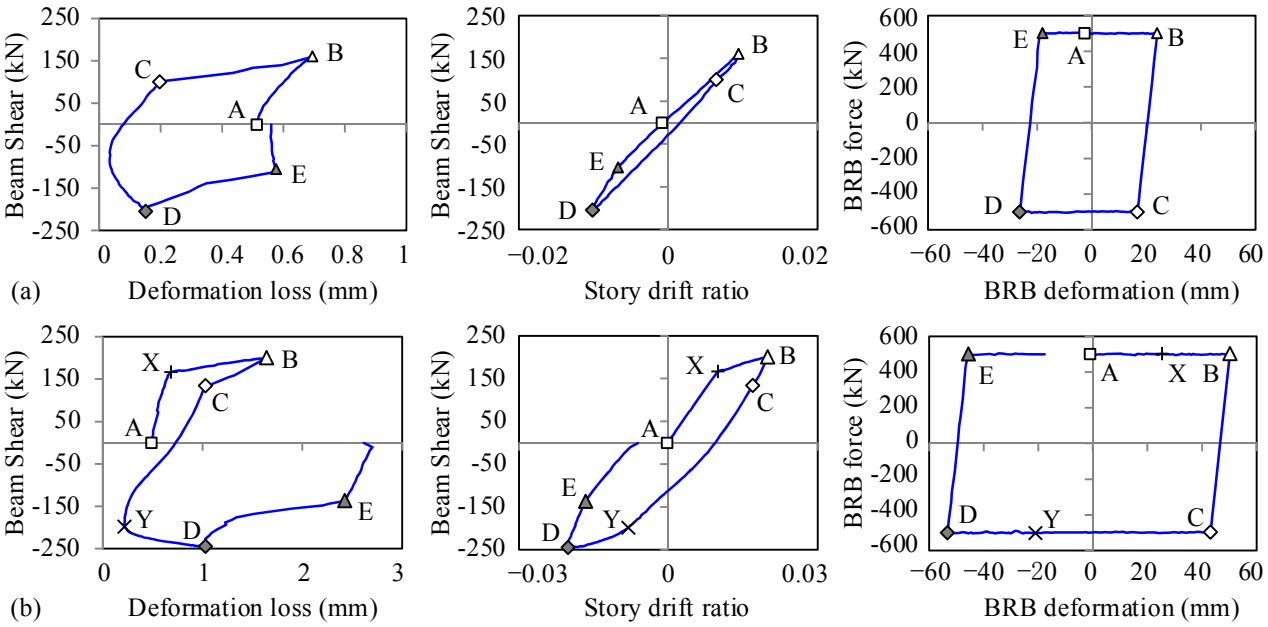

FIG. 9. Development of deformation loss at gusset connection of Specimen No.2, PT: (a) 1/100 load cycle and (b) 1/50 load cycle.

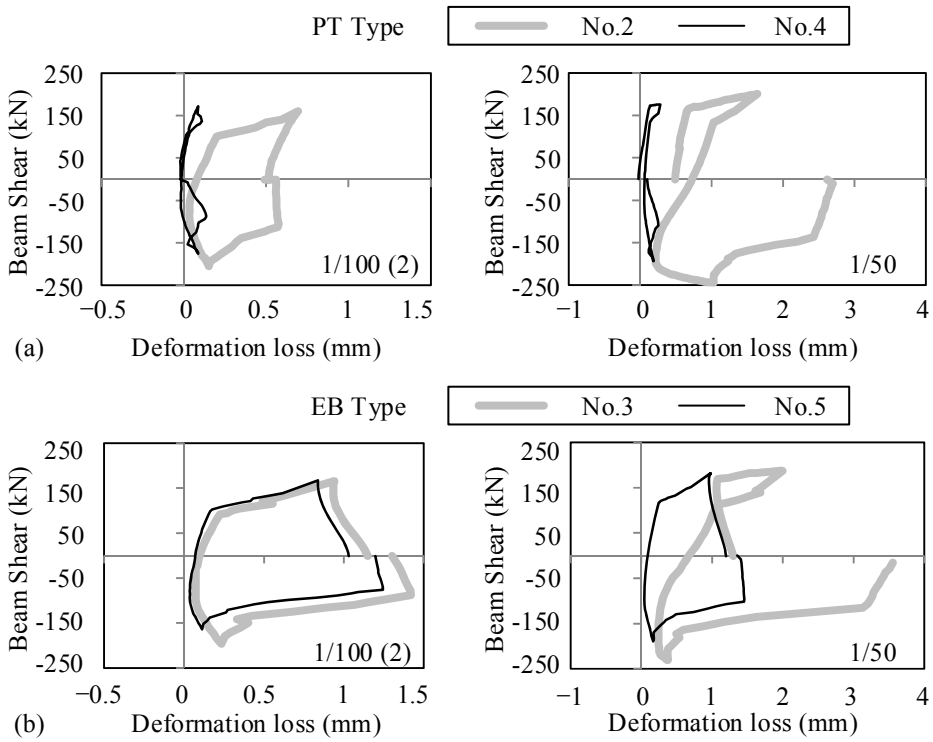

FIG. 10. Deformation loss at gusset connection: (a) Specimen No.2 and No.4, PT type and (b) No.3 and No.5, EB type connection.

The deformation loss indicates a reduction in the energy dissipation of the BRB. An 'energy ratio' can be defined as the ratio of the BRB's actual hysteretic energy in a complete load cycle of a given story drift amplitude, E, to the hysteretic energy that would have been dissipated if the connection is rigid, E_0 for the same story drift amplitude. As can be seen in Figure 11, the energy ratio generally increases for larger story drift amplitudes. This implies that as the story drift increases, the BRB's effective deformation grows faster than the deformation loss does. In addition, the energy ratios for the PT specimens are generally larger than those for the EB specimens, indicating larger stiffness of the PT connections. The damage control also had an effect on the energy ratios but in different ways for the PT and the EB

specimens. With the DC scheme, the energy ratio of Specimen No.4 was larger than that of No.2, especially when the story drift was small (Figure 11(a)). In contrast, the energy ratios of Specimen No.3 and No.5 were almost the same for small story drifts, but a considerable decrease in the energy ratio was observed for Specimen No.3 at 1/50 story drift (Figure 11(b)), when the RC beam segment surrounding the embedded gusset plate was severely damaged. Nevertheless, for all specimens in the test, the energy ratios were above 90% throughout the loading history. Such a less-than-10% reduction in the BRB's energy dissipation is not likely to bring about safety issues, and is negligible compared with the much greater uncertainties associated with the earthquake input.

Gusset slip

The slip of the gusset plate along the connection interface was monitored by an LVDT during the test, denoted as δ_S in Figure 8. Such a slip may compromise the initial gap intended to separate the gusset plate and the RC column. In Specimen No.3 (EB), the measured gusset slip, δ_S, reached as large as 5.83 mm towards the column during the 1/50 load cycle, while that of the other braced specimens remained below 2 mm. If such slip took place while the gusset plate was rotated with the beam end towards to column, the gusset plate would possibly touch the column at story drift ratio much smaller than intended. Fortunately, this was not the case for the present application. As can be seen in Figure 12, in which the definitions of Point A ~ E and Y are the same as those in Figure 9, the gusset slip, δ_S, towards the column (positive in value) reached its maximum near Point D when the BRB was in compression but the gusset plate was rotating together with the RC beam end away from the column. In such cases, the gusset plate would not touch the column as long as the slip is smaller than the initial gap. On the other hand, Point C seems to represent a critical state for the gusset plate to touch the column because the gusset plate was rotated towards the column and meanwhile the BRB was in compression. Nevertheless, the gusset slip at Point C was negligible, and thus the impairment to the initial gap was only marginal.

The damage control scheme made a significant difference in mitigating the gusset slip in the EB type specimens. In Specimen No.3, where the RC beam segment right beneath the gusset plate was severely damaged, the gusset slip increased rapidly after the RC beam yielded at Point Y. This was, however, not observed in the counterpart Specimen No.5, in which the damage control scheme was applied.

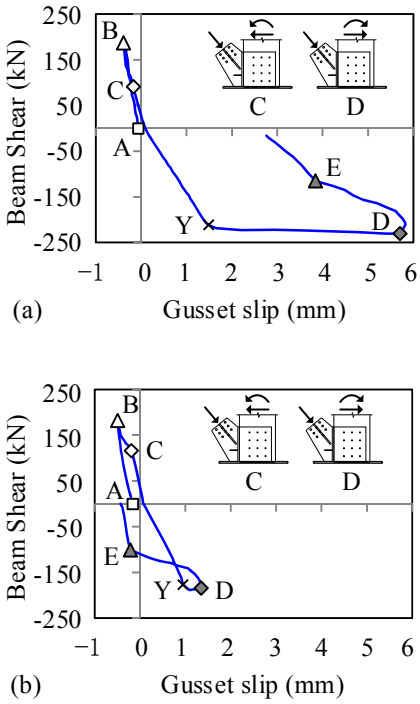

FIG. 12. Gusset slip during 1/50 load cycle: (a) Specimen No.3 and (b) No.5.

After the load cycle of 1/50 story drift ratio was completed, the beams were pushed monotonically towards the positive direction until the stroke of the horizontal actuators ran out, while the BRB force was kept constant at 500 kN in tension. As a result, all specimens were loaded to larger than 1/20 story drift ratios and the gusset plate did not touch the column (i.e., the stub) throughout the loading with the exception of Specimen No.3, in which the edge of the gusset plate bit into the RC stud top surface at 1/20 story drift (Figure 13). Such penetration is not likely a result of the gusset slip with respect to the RC beam, δ_S, because it was negligibly small during the positive loading as discussed above. Rather, it is more a consequence of the severe concrete crushing at the toe of the RC beam end (Figure 13b), which was not observed in the other specimens.

Embedded stud connections

Compared with the PT type connections, in which the local resistance can be clearly decomposed into a tangent and a normal component on the gusset-to-concrete interface, the EB type connections subject the embedded stud groups to a complex combination of diagonal shear force and eccentric moment.

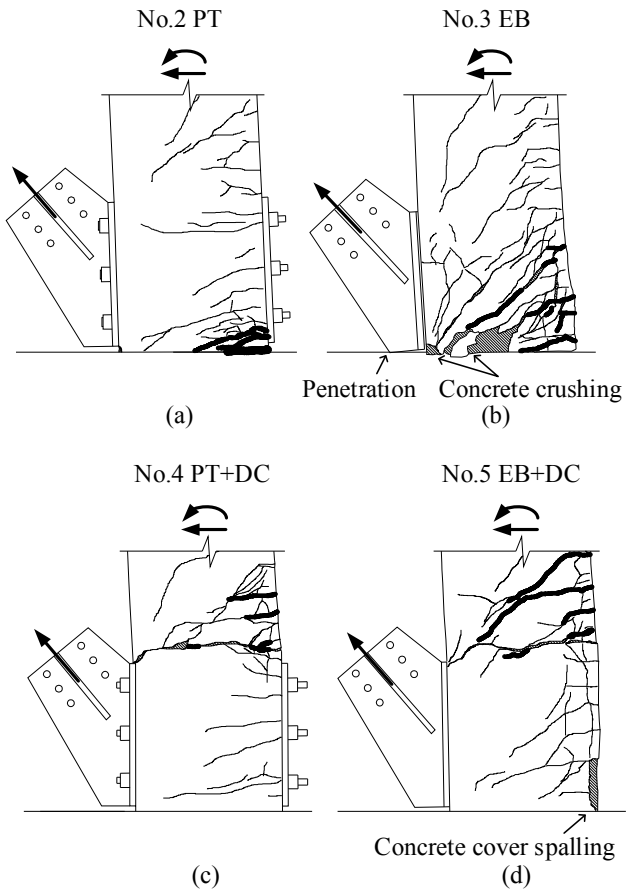

FIG. 13. Deformed shape of RC beam end at 1/20 story drift of (a) Specimen No.2, (b) No.3, (c) No.4 and (d) No.5.

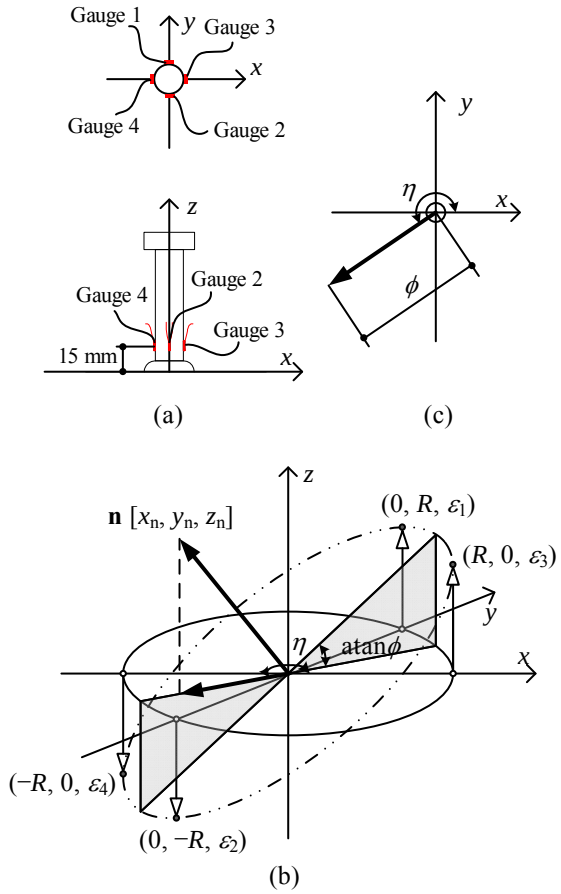

FIG. 14. Calculation of curvature at end of stud from strain readings.

The curvature at the cross section close to the bottom of each stud was measured by four strain gauges as shown in Figure 14(a). The gauges were attached 15 mm away from the plate surface to give way to the welds. Although the stud may have experienced plasticity and thus the curvature was not proportional to the moment carried by the stud, and the shear deformation of the studs cannot be captured by such measurements, the distribution of the measured curvatures provides a rough estimate of the shear force distribution of the stud group.

If the stud's cross section remains plane and the strain measurement is accurate, the four points defined by the gauge coordinates and the corresponding strain readings would lie in the same inclined 'strain plane' as shown in Figure 14(b). The normal vector of the strain plane, $\mathbf{n}(x_n, y_n, z_n)$, can be found. The magnitude of the curvature, ϕ, can be taken as the tangent of the inclination angle of the strain plane with respect to the original cross section plane, which is given in Equation (8) through the coordinates of the vector **n**. The projection of **n** on the original cross section plane, $(x_n, y_n, 0)$ gives the curvature direction, η. In such a manner, both the magnitude and the direction of the curvature can be worked out for each stud as shown in Figure 14(c).

In reality, however, a strain plane can be uniquely determined by each three out of the four stain readings and the so-determined four strain planes do not perfectly coincide with each other. Hence, the four sets of parameters of the strain planes defined by different sets of strain gauges were averaged for the curvature evaluation. There were also cases that a strain gauge on a stud might fail or yield unreliable results at a certain point during the loading so that only one strain plane can be determined by the rest three strain readings. In rare cases, two out of the four gauges failed to yield reliable results so that a strain plane cannot be found. This happened to only one out of the 24 instrumented studs of the two EB type specimens in the present test.

$$\phi = \frac{\sqrt{x_n^2 + y_n^2}}{|z_n|} \tag{8}$$

Figure 15 and 16 summarize the results of the measured curvatures for the EB type connections, where the arrow lengths indicate the curvature magnitudes. During the 1/100 load cycle when the RC beam ends only slightly yielded, the stud groups in both specimens exhibited similar curvature distributions. When the BRB was in its maximum tension (e.g., at the peak point B and the unloading.

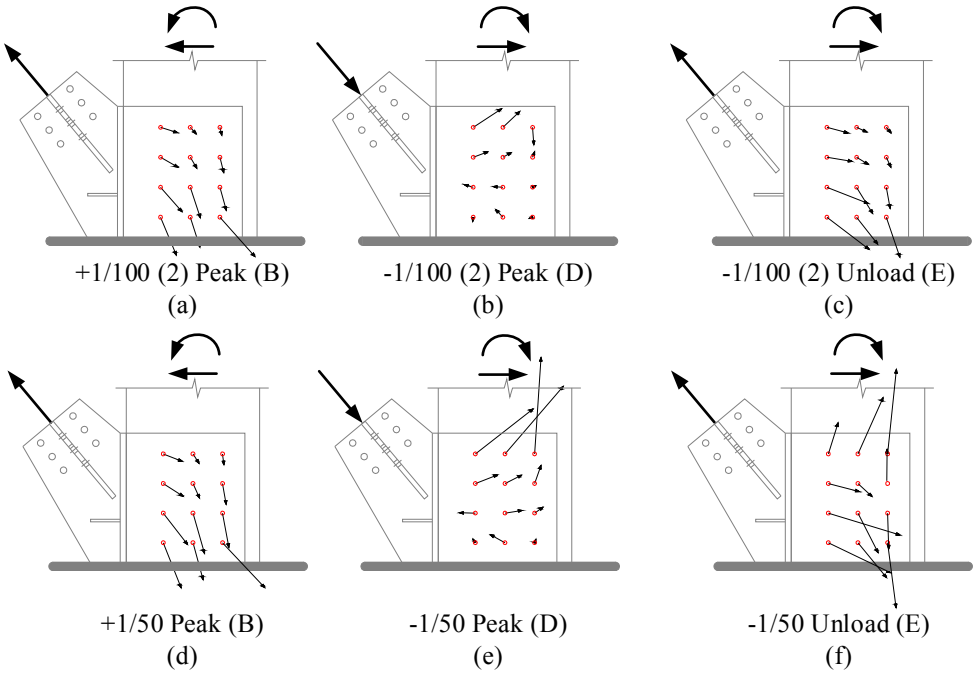

FIG. 15. Direction and magnitude of curvature at stud ends of Specimen No.3 (EB).

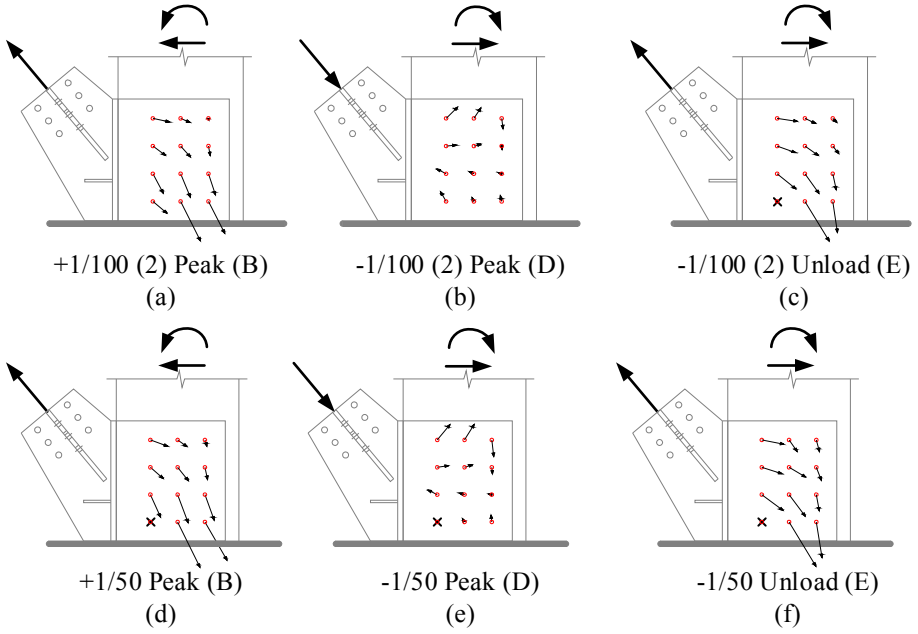

FIG. 16. Direction and magnitude of curvature at stud ends of Specimen No.5 (EB+DC).

point E, see Figure 9 for reference although it is for a different specimen), the curvatures of all studs in the group were generally in the opposite direction of the BRB axial force and the curvature magnitudes were much larger in the studs closer to the axis of BRB force. This was not much affected by the internal force in the RC beam, as can be seen in the comparison of (a) and (c) in either Figure 15 or Figure 16. When the BRB was in compression (e.g., at the negative peak point D), the stud curvatures became much smaller because the base plate of the gusset plate resisted much of the BRB compressive force.

The stud groups in the two specimens exhibited quite different curvature distributions when they were further loaded to 1/50 story drift, at which the RC beam ends sustained considerable damage and the DC scheme began to make a difference. At point B when BRB was in tension and the RC beam end was in positive loading, the stud curvatures of Specimen No.3 (Figure 15(d)) were similar to those during the 1/100 load cycle. This was, however, significantly altered when the RC beam was subjected to negative loading (Figure 15(f)). In particular, four studs near the top edge of the embedded plate exhibited large curvatures in the direction along the RC beam axis

and opposite to the others. Similar phenomenon can be observed when the RC beam was loaded negatively and the BRB was in compression (i.e., at point D, Figure 15(e)). It appears that the negative moment at the beam cross section tended to tear the stud group apart along major cracks that went into the region of embedment, as shown in Figure 7.

In contrast, the disturbed distribution of stud curvatures at the studs close to the upper edge of the embedded plate was not observed for Specimen No.5 (EB + DC) throughout the loading. Instead, the distribution of stud curvatures in No.5 remained almost the same in the 1/50 load cycle as it was in the 1/100 load cycle (Figure 16). This is consistent with the fact that no major cracks have gone into the embedment region because the damage control scheme successfully moved the plastic hinge out of the connection region.

CONCLUSIONS

An unconstrained gusset connection was proposed for buckling restrained braces in RC frames, in which the BRB gusset plate is separated from the RC column by an intended gap in order to make the load conditions of both the column and the connection clearer. Rearrangement of the rebars in the RC beam that receives the gusset connection was also proposed to control the local damage that may impair the reliability of the gusset connection. Specifically, additional rebars were provided for the connection region while the number of rebars was reduced outside the region to ensure that the potential plastic hinge of the RC beam is located outside the critical region.

Cyclic loading test on RC beam-gusset connection subassemblies was conducted to verify the proposal. Focus has been given to the effect of the proposed damage control scheme. From the test results and the above discussions, the following conclusions can be drawn.

(1) In addition to eliminating the impairment to the RC column, it is possible to minimize the influence of the unconstrained gusset connection on the performance of the RC beam by adjusting the flexural strength of the beam section to relocate the potential plastic hinge to outside the connection region. Besides, the BRBs generally begin to sustain plastic deformation at much smaller story drift (less than 1/500) than the RC beam does (around 1/100), even if the deformation loss at the gusset connection is taken into account. This ensures the advantage of BRBs to dissipate energy and reduce the global seismic response before the RC frame sustains considerable damage.

(2) The design for the local damage control at the RC beam end was effective in moving the potential plastic hinge to outside the connection region, as confirmed by the observed crack pattern on the beam surface and the strain readings of the beam longitudinal bars. A significant benefit of doing so is to prevent the BRBs from dislocating from the rest of the structure in case the beam fails in extreme earthquake events.

(3) The test results proved that the nonlinear deformation of the beam has an effect on the deformation loss especially when the beam end sustained considerable damage. This effect is more significant in the EB type connections than the PT type ones. However, the reduction in the BRB's energy dissipation associated with the deformation loss is less than 10% and practically negligible.

Besides, while both the EB and the PT type connections are available choices if properly designed, the latter has the advantages of clearer load condition and the possibility of being implemented in seismic retrofit of existing buildings.

ACKNOWLEDGEMENT

This research was funded by the National Natural Science Foundation of China for Young Scholars (No.51308514), the International Science & Technology Cooperation Program of China (No.2014DFA70950) and a collaborative research project provided by Structural Engineering Research Center at Tokyo Tech (No.219). The financial support is gratefully appreciated. The authors are also grateful to Mr. Toshio Maegawa and Mr. Makoto Hamada of Kumagai Gumi Co., Ltd. for their help in preparing and conducting the tests.

REFERENCES

AISC (American Institute of Steel Construction). (2010). "Prequalified connections for special and intermediate steel moment frames for seismic applications." *ANSI/AISC 358-10*, Chicago, 11-15.

Baltay, P., and Gjelsvik, A. (1990). "Coefficient of friction for steel on concrete at high normal stress". *J. Mater. Civ. Eng.*, 10.1061/(ASCE)0899-1561(1990)2:1(46), 46-49.

Bentz, E.C. (2000). *Sectional Analysis of Reinforced Concrete*, Ph.D. Thesis, Department of Civil Engineering, University of Toronto, Toronto, Canada.

Berman, J.W., and Bruneau, M. (2009). "Cyclic testing of a buckling restrained braced frame with unconstrained gusset connections." *J. Struct. Eng.*, 10.1061/(ASCE)ST.1943-541X.0000078, 1499-1510.

Brown, A.P., Aiken, I.D., and Jafarzadeh, F.J. (2001). "Buckling restrained braces provide the key to the seismic retrofit of the Wallace F. Bennett Federal Building". *Modern Steel Construction*, Aug.

Gu, L.Z., Gao, X.Y., Xu, J.W., and Na, W. (2011). "Research on seismic performance of BRB concrete frames." *Journal of Building Structures*, 32(7), 101-111 (in Chinese).

Harayama, K., Kawamoto, T., Inai, E., and Matsukane, Y.

(2012). "An experimental study of a seismic retrofitting method with framed steel brace systems partially and concentrically jointed with anchors." *Proc. 15th World Conference on Earthquake Engineering*, <http://www.iitk.ac.in/nicee/wcee/article/WCEE2012_1846.pdf> (Mar. 16, 2015).

Ishimura, M., Sadasue, K., Fujii, T., Yokoyama, T., Minami, K. (2011). "Seismic retrofitting steel brace which uses post-installed anchor together with expxy resin for RC structures with low-strength concrete." *Journal of Structural and Construction Engineering, Transaction of AIJ*, 76(659), 141-148 (in Japanese).

Ishii, T., Mukai, T., Kitamura, H., Shimizu, T., Fujisawa, K., and Ishida, Y. (2004). "Seismic retrofit for existing R/C building using energy dissipative braces". *Proc. 13th World Conference on Earthquake Engineering*, <http://www.iitk.ac.in/nicee/wcee/article/13_1209.pdf> (Mar. 16, 2015).

Ishimura, M., Sadasue, K., Miyauchi, Y., Yokoyama, T., Fujii, T., Minami, K. (2012). "Seismic performance evaluation for retrofitting steel brace of existing RC buildings with low-strength concrete". *Proc. 15th World Conference on Earthquake Engineering*, <http://www.iitk.ac.in/nicee/wcee/article/WCEE2012_0412.pdf> (Mar. 16, 2015).

Jones, S.L., Fry, G.T., and Engelhardt, M.D. (2002). "Experimental evaluation of cyclically loaded reduced beam section moment connections." *J. Struct. Eng.*, 10.1061/(ASCE)0733-9445(2002)128:4(441), 441-451.

JSSI (The Japan Society of Seismic Isolation). (2007). *Manual for design and construction of seismically passive controlled building structures (2nd Edition)*, Tokyo, Japan (in Japanese).

Kisiki, S., Yamada, S., and Wada, A. (2008). "Experimental evaluation of structural behavior of gusset plate connection in BRB frame system." *Proc. 14th World Conference on Earthquake Engineering*, <http://www.iitk.ac.in/nicee/wcee/article/14_05-05-0004.pdf> (Mar. 16, 2015)

Ogawa, Y., Isoda, K., Kitamura, Y., and Yasuo, J. (2004). "Experimental study on the structural properties of high strength reinforced concrete frames with brace dampers." *Summaries of technical papers of AIJ annual meeting*, Architectural Institue of Japan, Tokyo, 1227-1230 (in Japanese).

Ollgaard, J.G., Slutter, R.G., Fisher, J.W. (1971). "Shear strength of stud connectors in lightweight and normal-weight concrete." *Engineering Journal of American Institute of Steel Construction*, 8(2), 55-64.

Rabbat, B.G., and Russell, H.G. (1985). "Friction coefficient of steel on concrete or grout." *J. Struct. Eng.*, 10.1061/(ASCE)0733-9445(1985)111:3(505), 505-515.

Watanabe, A., Hitomi, Y., Saeki, E., Wada, A., and Fujimoto, M. (1988). "Properties of brace encased in buckling-restraining concrete and steel tube." *Proc. 9th World Conference on Earthquake Engineering*, < http://www.iitk.ac.in/nicee/wcee/article/9_vol4_719.pdf > (Mar. 16, 2015).

Yokouchi, H., Kitajima, K., Ageta, H., Chikui, H., Nakanishi, M., and Adachi, H. (2004). "Pseudo-dynamic test on an existing R/C school building retrofitted with friction dampers." *Proc. 13th World Conference on Earthquake Engineering*, <http://www.iitk.ac.in/nicee/wcee/article/13_2111.pdf> (Mar. 16, 2015).